ICE–OCEAN INTERACTION

J. H. Morison, University of Washington, Seattle, WA, USA
M. McPhee, McPhee Research Company, Naches, WA, USA

doi:10.1006/rwos.2001.0003

Introduction

The character of the sea ice cover greatly affects the upper ocean and vice versa. In many ways ice-covered seas provide ideal examples of the planetary boundary layer. The under-ice surface may be uniform over large areas relative to the vertical scale of the boundary layer. The absence of surface waves simplifies the boundary layer processes. However, thermodynamic and mechanical characteristics of ice–ocean interaction complicate the picture in unique ways. We discuss a few of those unique characteristics.

We deal first with how momentum is transferred to the water and introduce the structure of the boundary layer. This will lead to a discussion of the processes that determine the fluxes of heat and salt. Finally, we discuss some of the unique characteristics imposed on the upper ocean by the larger-scale features of a sea ice cover.

Drag and Characteristic Regions of the Under-ice Boundary Layer

To understand the interaction of the ice and water, it is useful to consider three zones of the boundary layer: the molecular sublayer, surface layer, and outer layer (**Figure 1**). Under a reasonably smooth and uniform ice boundary, these can be described on the basis of the influence of depth on the terms of the equation for a steady, horizontally homogeneous boundary layer (eqn [1]).

$$if\,V = \frac{\partial}{\partial z}\left(\nu\frac{\partial V}{\partial z}\right) + \frac{\partial}{\partial z}\left(K\frac{\partial V}{\partial z}\right) - \rho^{-1}\nabla_h p \qquad [1]$$

The coordinate system is right-handed with z positive upward and the origin at the ice under-surface. V is the horizontal velocity vector in complex notation ($V = u + iv$), ρ is water density, and p is pressure. An eddy diffusivity representation is used for turbulent shear stress, $K(\partial V/\partial z) = \overline{V'w'}$, where K is the eddy diffusivity. The term $\nu(\partial V/\partial z)$ is the viscous shear stress, where ν is the kinematic molecular viscosity. The pressure gradient term, $\rho^{-1}\nabla_h p$ is equal to $\rho^{-1}(\partial p/\partial x + i\partial p/\partial y)$.

The stress gradient term due to molecular viscosity is of highest inverse order in z. It varies as z^{-2}, and therefore dominates the stress balance in the molecular sublayer (**Figure 1**) where z is vanishingly small. As a result the viscous stress, $\nu(\partial V/\partial z)$, is effectively constant in the molecular sublayer, and the velocity profile is linear.

The next layer away from the boundary is the surface layer. Here the relation between stress and velocity depends on the eddy viscosity, which is proportional to the length scale and velocity scale of turbulent eddies. The length scale of the turbulent eddies is proportional to the distance from the boundary, $|z|$. Therefore, the turbulent stress term varies as z^{-1} and becomes larger than the viscous term beyond z greater than $(1/k)(\nu/u_{*0})$, typically a fraction of a millimeter. The velocity scale in the surface layer is u_{*0}, where ρu_{*0}^2 is equal to τ_0, the average shear stress at the top of the boundary layer. Thus, K is equal to $ku_{*0}|z|$, where Von Kärmän's constant, k, is equal to 0.4. Because the turbulent stress term dominates the equations of motion, the stress is roughly constant with depth in the surface layer. This and the linear z dependence of the eddy coefficient result in the log-layer solution or 'law of the wall' (eqn [2]).

$$\frac{u}{u_*} = \frac{1}{k}\ln z + C = \frac{1}{k}\ln\frac{z}{z_0} \qquad [2]$$

$C = -(\ln z_0)/k$ is a constant of integration. Under sea ice the surface layer is commonly 1–3 m thick.

The surface layer is where the influence of the boundary roughness is imposed on the planetary boundary layer. In the presence of under-ice roughness, the average stress the ice exerts on the ocean, τ_0, is composed partly of skin friction due to shear and partly of form drag associated with pressure disturbances around pressure ridge keels and other roughness elements. Observations under very rough ice have shown a decrease in turbulent stress toward the surface, presumably because more of the momentum transfer is taken up by pressure forces on the rough surface. The details of this drag partition are not known. Drag partition is complicated further for cases in which stratification exists at depths

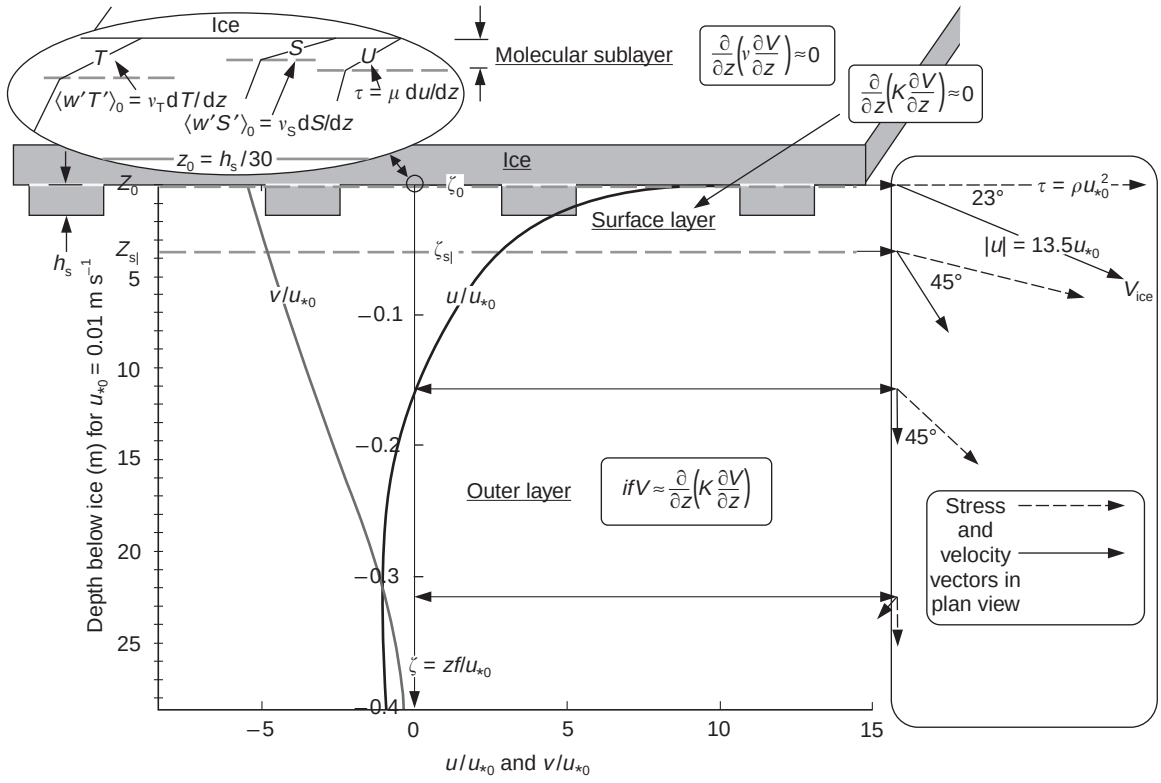

Figure 1 Illustration of three regions of the planetary boundary layer under sea ice: molecular sublayer, surface layer, and outer layer. The velocity profiles are from the Rossby similarity solution (eqns [8], [9], [10] and [11]) for $u_{*0} = 0.01\,\mathrm{m\,s^{-1}}$, $z_0 = 0.06\,\mathrm{m}$, $\eta_* = 1$. The stress and velocity vector comparisons are from the same solution.

shallow compared to the depth of roughness elements. Then it also becomes possible to transfer momentum by internal wave generation. However, for many purposes τ_0 is taken as the turbulent stress evaluated at z_0. Laboratory studies of turbulent flow over rough surfaces suggest that z_0 may be taken equal to $h_s/30$, where h_s is the characteristic height of the roughness elements.

In rare situations the ice surface may be so smooth that bottom roughness and form drag are not factors in the drag partition. In such a hydrodynamically smooth situation, the turbulence is generated by shear induced instability in the flow. The surface length scale, z_0, is determined by the level of turbulent stress and is proportional to the molecular sublayer thickness according to the empirically derived relation $z_0 = 0.13(\nu/u_{*0})$.

In the outer layer farthest from the boundary, the Coriolis and pressure gradient terms in eqn [1], which have no explicit z dependence, are comparable to the turbulent stress terms. The presence of the Coriolis term gives rise to a length scale, h, for the outer boundary layer equal to u_{*0}/f under neutral stratification. This region is far enough from the boundary so that the turbulent length scale becomes independent of depth and in neutral conditions has been found empirically to be $\lambda = \xi_n u_{*0}/f$, where ξ_n is 0.05. For neutral stratification, u_* and h are the independent parameters that define the velocity profile over most of the boundary layer. The ratio of the outer length scale to the surface region length scale, z_0, is the surface friction Rossby number, $R_0 = u_{*0}/(z_0 f)$.

Solutions for the velocity in the outer layer can be derived for a wide range of conditions if we nondimensionalize the equations with these Rossby similarity parameters, u_{*0}/f and u_{*0}. However, the growth and melt of the ice produce buoyancy flux that strongly affects mixing. Melting produces a stabilizing buoyancy flux that inhibits turbulence and contracts the boundary layer. Freezing causes a destabilizing buoyancy flux that enhances turbulence and thickens the boundary layer. We can account for the buoyancy flux effect by adjusting the Rossby parameters dealing with length scale. We define the scale of the outer boundary layer as $h_m = u_{*0}\eta_*/f$. If the mixing length of the turbulence in the outer layer is $\lambda_m = \xi_n u_{*0}\eta_*^2/f$, it interpolates in a reasonable way between known values of λ_m for neutral stratification $(\xi_n u_{*0}/f)$

and stable stratification (R_cL) if η_* is given as eqn [3].

$$\eta_* = \left(1 + \frac{\xi_n u_*}{f}\frac{1}{R_c L}\right)^{1/2} \quad [3]$$

R_c is the critical Richardson number; the Obukhov length, L, is the ratio of shear and buoyant production of turbulent energy, $\rho u_{*0}^3/kg\langle\rho'w'\rangle$; and $-\langle\rho'w'\rangle g/\rho$ is the turbulent buoyancy flux. With this Rossby similarity normalization of the equations of motion, we can derive analytical expressions for the under-ice boundary layer profile that are applicable to a range of stratification.

For large $|z|$, V will approach the free stream geostrophic velocity, $\bar{V}_g = U_g + iV_g = f^{-1}\rho^{-1}\nabla_h p$. Here we will assume this is zero. However, surface stress-driven absolute velocity solutions can be superimposed on any geostrophic current. We also ignore the time variation and viscous terms and define a normalized stress equal to $\Sigma = (K\partial V/\partial z)/u_{*0}^2$. The velocity is nondimensionalized by the friction velocity and the boundary layer thickness, $U = Vfh_m/u_{*0}^2$, and depth is nondimensionalized by the boundary layer thickness scale, $\zeta = z/h_m$. With these changes eqn [1] becomes eqn [4].

$$iU = \partial\Sigma/\partial\zeta \quad [4]$$

In terms of nondimensional variables the constitutive law is given by eqn [5].

$$\Sigma = K_*\partial U/\partial\zeta \quad [5]$$

The nondimensional eddy coefficient is given by eqn [6].

$$K_* = ku_{*0}\lambda_m/fh_m^2 = k\xi_n \quad [6]$$

Eqn [6] is the Rossby similarity relation that is the key to providing similarity solutions for stable and neutral conditions. It even provides workable results for slightly unstable conditions.

Eqns [4] and [5] can be combined in an equation for nondimensionalized stress (eqn [7]).

$$(i/K_*)\Sigma = d\Sigma/d\zeta \quad [7]$$

This has the solution eqn [8].

$$\Sigma = e^{\hat{\delta}\zeta} \quad [8]$$

$$\hat{\delta} = (i/K_*)^{1/2} \quad [9]$$

Eqn [8] attenuates and rotates (to the right in the Northern Hemisphere) with depth. It duplicates the salient features found in data and sophisticated numerical models.

In the outer layer, eqns [5] and [8] are satisfied for nondimensional velocity given by eqn [10].

$$U = -i\hat{\delta}e^{\hat{\delta}\zeta} \quad \text{for } \zeta \le \zeta_0 \quad [10]$$

Thus the velocity is proportional to stress but rotated 45° to the right.

As we see in the derivation of the law of the wall [2], the surface layer variation of the eddy viscosity with depth is critical to the strong shear present there. Thus eqn [10] will not give a realistic profile in the surface layer. We define the nondimensional surface layer thickness, ζ_{sl}, as the depth where the surface layer mixing length, $|z|$, becomes equal to the outer layer mixing length, $\lambda_m = \xi_n u_{*0}\eta_*^2/f$. We find ζ_{sl} is equal to $-\eta_*\xi_n$ and applying the definition [6] gives K_* as $K_{*sl} = -k\zeta/\eta_*$ in the surface layer. If we approximate the stress profile [8] by a Taylor series, we can integrate [5] with K_{*sl} substituted for K_* to obtain the velocity profile in the surface layer.

$$U(\zeta) - U(\zeta_{sl}) = \frac{\eta_*}{k}\left[\ln\left(\frac{\zeta_{sl}}{\zeta_0}\right) + \hat{\delta}(\zeta_{sl} - \zeta)\right] \quad \text{for } \zeta \ge \zeta_0 \quad [11]$$

Eqn [11] is analogous to [2] except for the introduction of the $\hat{\delta}(\zeta_{sl} - \zeta)$ term. This is the direct result of accounting for the stress gradient in the surface layer. This term is small compared to the logarithmic gradient.

Figure 1 illustrates the stress and velocity vectors at various points in the boundary layer as modeled by eqns [8] through [11]. For neutral conditions the nondimensional boundary layer thickness is typically 0.4 (dimensional thickness is $0.4u_*/f$). Through the outer layer, the velocity vector is 45° to the right of the stress vector as a consequence of the $-i\hat{\delta} \propto e^{-i(45°)}$ multiplier in [10]. As the ice surface is approached through the surface layer, the stress vector rotates 10–20° to the left to reach the surface direction. However, in the surface layer the velocity shear in the direction of the surface stress is great because of the logarithmic profile. Thus, as the surface is approached, the velocity veers to the left twice as much as stress. At the surface the velocity is about 23° to the right of the surface stress.

It is commonly useful to relate the stress on under-ice surface to the relative velocity between ice and water a neutral-stratification drag coefficient,

$\rho u_{*0}^2 = \rho C_z V_{(z)}^2$ where C_z is the drag coefficient for depth z. If z is in the log-layer, eqn [2] can be used to derive the relation between ice roughness and the drag coefficient. We find that $C_z = k^2[\ln(z/z_0)]^{-2}$. Clearly values of the drag coefficient can vary widely depending on the under-ice roughness. Typical values of z_0 range from 1 to 10 cm under pack ice. A commonly referenced value for the Arctic is 6 cm, which produces a drag coefficient at the outer edge of the log layer of 9.4×10^{-3} (**Figure 1**).

If the reference depth is outside the log layer, the drag coefficient formulation is poorly posed because of the turning in the boundary layer. For neutral conditions, eqns [10] and [11] can be used to obtain a Rossby similarity drag law that yields the nondimensional surface drift relative to the geostrophic current for unit nondimensional surface stress (eqn [12]).

$$U_0 = \frac{V_0}{u_{*0}} = \frac{1}{k}([\ln(R_0) - A] - iB) \qquad [12]$$

Here

$$A = \left(1 - \ln \xi_n - \sqrt{\frac{k}{2\xi_n}} + \sqrt{\frac{\xi_n}{2k}}\right) \cong 2.2$$

$$B = \sqrt{\frac{k}{2\xi_n}} + \sqrt{\frac{\xi_n}{2k}} \cong 2.3 \qquad [13]$$

This Rossby similarity drag law for outside the surface layer results in a surface stress that is proportional to $V^{1.8}$ rather than V^2, a result that is supported by observational evidence, and can be significant at high velocities.

Heat and Mass Balance at the Ice–Ocean Interface: Wintertime Convection

The energy balance at the ice–ocean interface not only exerts major influence over the ice mass balance but also dictates the seasonal evolution of upper ocean salinity and temperature structure. At low temperature, water density is controlled mainly by salinity. Salt is rejected during freezing, so that buoyancy flux from basal growth (or ablation), combined with turbulent mixing during storms, determines the depth of the well-mixed layer.

Vertical motion of the ice–ocean interface depends on isostatic adjustment as the ice melts or freezes. The interface velocity is $w_0 + w_i$ where $w_0 = -(\rho_{ice}/\rho)\dot{h}_b, \dot{h}_b$ is the basal growth rate, and w_i represents isostatic adjustment to runoff of surface melt and percolation of water through the ice cover. In an infinitesimal control volume following the ice–ocean interface, conservation of heat and salt may be expressed in kinematic form as eqns [14] and [15].

$$\dot{q} = \langle w'T' \rangle_0 - w_0 Q_L \ (\text{with units K m s}^{-1}) \qquad [14]$$

$$(w_0 + w_i)(S_0 - S_{ice}) = \langle w'S' \rangle_0 \ (\text{with units psu m s}^{-1}) \qquad [15]$$

where $\dot{q} = H_{ice}/(\rho c_p)$ is flux (H_{ice}) conducted away from the interface in the ice; ρ is water density; c_p is specific heat of seawater; $\langle w'T' \rangle_0$ is the kinematic turbulent heat flux from the ocean; Q_L is the latent heat of fusion (adjusted for brine volume) divided by c_p; S_0 is salinity in the control volume, S_{ice} is ice salinity, and $\langle w'S' \rangle_0$ is turbulent salinity flux. Fluid in the control volume is assumed to be at its freezing temperature, approximated by the freezing line (eqn [16]).

$$T_0 = -mS_0 \qquad [16]$$

By standard closure, turbulent fluxes are expressed in terms of mean flow properties (eqns [17] and [18]).

$$\langle w'T' \rangle_0 = c_h u_{*0} \delta T \qquad [17]$$

$$\langle w'S' \rangle_0 = c_S u_{*0} \delta S \qquad [18]$$

u_{*0} is the square root of kinematic turbulent stress at the interface (friction velocity); $\delta T = T - T_0$ and $\delta S = S - S_0$ are differences between far-field and interface temperature and salinity; and c_h and c_S are turbulent exchange coefficients termed Stanton numbers.

The isostatic basal melt rate, w_0 is the key factor in interface thermodynamics, and in combination with w_i it determines the salinity flux. A first-order approach to calculating w_0 that is often sufficiently accurate (relative to uncertainties in forcing parameters) when melting or freezing is slow, is to assume that $S_0 = S$, the far-field salinity, and that c_h is constant. Combining [14], [16], and [17] gives eqn [19].

$$w_0 = \frac{c_h u_{*0}(T + mS) - \dot{q}}{Q_L} \qquad [19]$$

Salinity flux is determined from [15]. Note the c_S is not used, and that this technique fixes (unrealistically)

the temperature at the interface to be the mixed layer freezing temperature.

A more sophisticated approach is required when melting or freezing is intense. Manipulation of [14] through [18] produces a quadratic equation for w_0 (eqn [20]).

$$\frac{S_L}{u_{*0}} w_0^2 + (S_T + S_L c_S - S_{ice}) w_0 + (u_{*0} c_S + w_i) S_T + u_{*0} c_S S - w_i S_{ice} = 0 \quad [20]$$

$$S_T = \left(\frac{\dot{q}}{c_h u_{*0}} - T \right) / m \quad \text{and} \quad S_L = Q_L / (m c_h) \quad [21]$$

Here c_h and c_S (turbulent Stanton numbers for heat and salt) are both important and not necessarily the same. Melting or freezing will decrease or increase S_0 relative to far-field salinity, with corresponding changes in T_0.

The Marginal Ice Zone Experiments (MIZEX) in the 1980s showed that existing ice–ocean turbulent transfer models overestimated melt rates by a wide factor. It became clear that the rates of heat and mass transfer were less than momentum transfer (by an order of magnitude or more), and were being controlled by molecular effects in thin sublayers adjacent to the interface. If it is assumed that the extent of the sublayers is proportional to the bottom roughness scale, z_0, then dimensional analysis suggests that the Stanton numbers (nondimensional heat and salinity flux) should depend mainly on two other dimensionless groups, the turbulent Reynolds number, $\mathrm{Re}_* = u_{*0} z_0 / \nu$, where ν is molecular viscosity, and the Prandtl (Schmidt) numbers, $\nu / \nu_{T(S)}$, where ν_T and ν_S are molecular diffusivities for heat and salt. Laboratory studies of heat and mass transfer over hydraulically rough surfaces suggested approximate expressions for the Stanton numbers of the form shown in eqn [22].

$$c_{h(S)} = \frac{\langle w' T(S)' \rangle_0}{u_{*0} \delta T(S)} \propto (\mathrm{Re}_*)^{-1/2} \left(\frac{\nu}{\nu_{T(S)}} \right)^{-2/3} \quad [22]$$

The Stanton number, c_h, has been determined in several turbulent heat flux studies since the original MIZEX experiment, under differing ice types with z_0 values ranging from less than a millimeter (eastern Weddell Sea) to several centimeters (Greenland Sea MIZ). According to [22], c_h should vary by almost a factor of 10. Instead, it is surprisingly constant, ranging from about 0.005 to 0.006, implying that the Reynolds number dependence from laboratory results cannot be extrapolated directly to sea ice.

If the Prandtl number dependence of [14] holds, the ratio $c_h / c_S = (\nu_h / \nu_S)^{2/3}$ is approximately 30. Under conditions of rapid freezing, the solution of [20] with this ratio leads to significant supercooling of the water column, because heat extraction far outpaces salt injection in what is called double diffusion. This result has caused some concern. Because the amount of heat represented by this supercooling is substantial, it has been hypothesized that ice may spontaneously form in the supercooled layer and drift upward in the form of frazil ice crystals. This explanation has not been supported by ice core sampling, which shows no evidence of widespread frazil ice formation beyond that at the surface of open water.

The physics of the freezing process suggest that the seeming paradox of the supercooled boundary layer may be realistic without spontaneous frazil formation. When a parcel of water starts to solidify into an ice crystal, energy is released in proportion to the volume of the parcel. At large scales this manifests itself as the latent heat of fusion. However, as the parcel solidifies, energy is also required to form the surface of the solid. This surface energy penalty is proportional to the surface area of the parcel and depends on other factors including the physical character of any nucleating material. In any event, if the parcel is very small the ratio of parcel volume to surface area will be so small that the energy released as the volume solidifies is less than the energy needed to create the new solid surface. For this reason, ice crystals cannot form even in supercooled water without a nucleating site of sufficient size and suitable character. In the clean waters of the polar regions, the nearest suitable site may only be at the underside of the ice cover where the new ice can form with no nucleation barrier. Therefore, it is possible to maintain supercooled conditions in the boundary layer without frazil ice formation.

Furthermore, recent results suggest that supercooling in the uppermost part of the boundary layer may be intrinsic to the ice formation process. Sea ice is a porous mixture of pure ice and high-salinity liquid water (i.e., brine). The bottom surface of a growing ice floe consists of vertically oriented pure ice platelets separated by vertical layers of concentrated brine. This platelet–brine sandwich (on edge) structure is on the scale of a fraction of a millimeter, and its formation is controlled by molecular diffusion of heat and salt. The low solid solubility of the salt in the ice lattice results in an increase of the salinity of water in the layer above the advancing freezing interface. Because heat diffuses more rapidly than salt at these scales, the cold brine tends to

supercool the water below the ice–water interface. With this local supercooling, any disturbance of the ice bottom will tend to grow spontaneously. The conditions of sea ice growth are such that this instability is always present. Continued growth results in additional rejection of salt, some fraction of which is trapped in the brine layers, and consequently the interfacial region of the ice sheet continues to experience constitutional supercooling. Also, anisotropy in the molecular attachment efficiency intrinsic to the crystal structure of the ice platelets creates an additional supercooling in the interfacial region. The net result is that heat is extracted from the top of the water column at the rate needed to maintain its temperature near but slightly below the equilibrium freezing temperature as salt is added. This and the convective processes in the growing ice may imply that $c_h/c_S = 1$ during freezing. The situation with melting may be quite different, since the physical properties of the interface change dramatically.

Observations to date suggest that c_h remains relatively unchanged with variable ice type and mixed layer temperature elevation above freezing. A value of 5.5×10^{-3} is representative. c_S is not so well known, since direct measurements of $\langle w'S' \rangle$ are relatively rare. The dependence of the exchange coefficients on Prandtl and Schmidt numbers is not clear, and will only be resolved with more research.

Effects of Horizontal Inhomogeneity: Wintertime Buoyancy Flux

Although the under-ice surface may be homogeneous over ice floes hundreds of meters in extent, the key fluxes of heat and salt are characteristically nonuniform. As ice drifts under the action of wind stress, the ice cover is deformed. Some areas are forced together, producing ridging and thick ice, and some areas open in long, thin cracks called leads. In special circumstances the ice may form large, unit-aspect-ratio openings called polynyas. In winter the openings in the ice expose the sea water directly to cold air without an intervening layer of insulating sea ice. This results in rapid freezing. As the ice forms, it rejects salt and results in unstable stratification of the boundary layer beneath open water or thin ice. These effects are so important that, even though such areas may account for less than 10% of the ice cover, they may account for over half the total ice growth and salt flux to the ocean. Thus the dominant buoyancy flux is not homogeneous but is concentrated in narrow bands or patches. Similarly, in the summer solar radiation is reflected from the ice but is nearly completely absorbed by open water. Fresh water from summertime surface melt tends to drain into leads, making them sources of fresh water flux as well.

The effect of wintertime convection in leads is illustrated in **Figure 2**. It shows two extremes in the upper ocean response. **Figure 2A** shows what we might expect in the case of a stationary lead. As the surface freezes, salt is rejected and forms more dense water that sinks under the lead. This sets up a circulation with fresh water flowing in from the sides near the surface and dense water flowing away from the lead at the base of the mixed layer.

Figure 2B illustrates the case in which the lead is embedded in ice moving at a velocity great enough to produce a well-developed turbulent boundary layer (e.g. $0.2\,\mathrm{m\,s^{-1}}$). If the mixed layer is fully turbulent, the cellular convection pattern may not occur; rather, the salt rejected at the surface may simply mix into the surface boundary layer.

The impact of nonhomogeneous surface buoyancy flux on the boundary layer can also be characterized by the equations of motion. The viscous terms in eqn [1] can be neglected at the scales we discuss here, but the possibility of vertical motion associated with large-scale convection requires that we include the vertical component of velocity. For steady state we have eqn [23].

$$\bar{V} \bullet \nabla \bar{V} + \bar{f} \times \bar{V} = \frac{\partial}{\partial z}\left(K \frac{\partial \bar{V}}{\partial}\right) - \rho^{-1} \nabla p \qquad [23]$$

$\bar{V}$ is the velocity vector including the mean vertical velocity w; $\bar{f}$ is the Coriolis parameter times the vertical unit vector. The advective acceleration term, $\bar{V} \bullet \nabla \bar{V}$, and pressure gradient term are necessary to account for the horizontal inhomogeneity that is caused by the salinity flux at the lead surface.

The condition that separates the free convection regime of **Figure 2A** and the forced convection regime of **Figure 2B** is expressed by the relative magnitude of the pressure gradient, $\rho^{-1} \nabla_h p$, and turbulent stress, $\partial/\partial z\,(K\,\partial V/\partial z)$, terms in [23]. This ratio can be derived with addition of mass conservation and salt conservation equations, and if we assume the vertical equation is hydrostatic, $\partial p/\partial z = -g\rho = -gMS$, where M is the sensitivity of density to salinity. If we nondimensionalize the equations by the ice velocity U_i, mixed-layer depth, d, average salt flux at the lead surface, F_S, and friction velocity, u_{*0}, the ratio of the pressure gradient term to the turbulent stress term scales as eqn [24].

$$L_0 = \frac{gMF_S d}{\rho_0 U_i u_{*0}^2} \qquad [24]$$

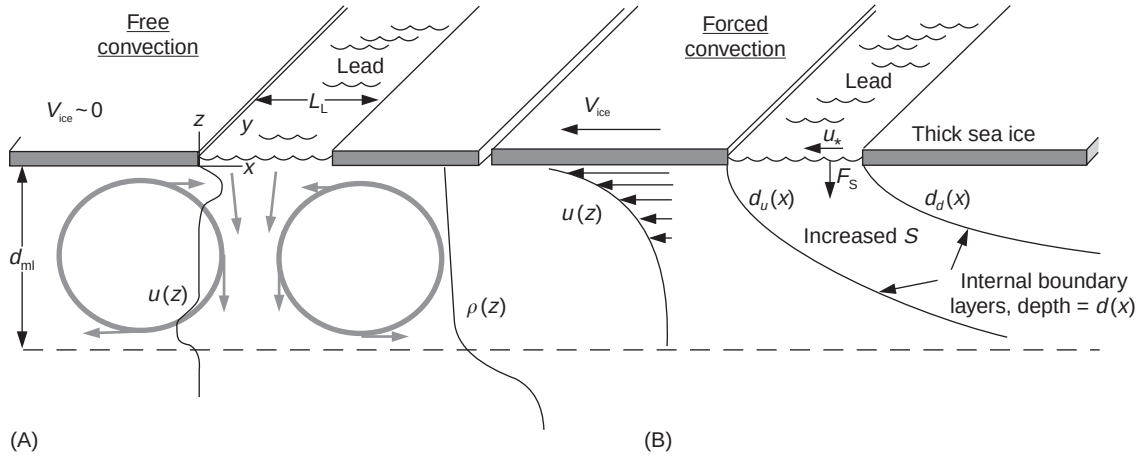

Figure 2 Modes of lead convection. (A) The free convection pattern that results when freezing and salt flux are strong, and the relative velocity of the ice is low. Cellular patterns of convective overturning are driven by pressure gradients that arise from the salinity disturbance due to ice formation. (B) The forced convection regime that exists when ice motion is strong. The salinity flux and change in surface stress in the lead cause a change in the character of the boundary layer that grows deeper downstream. The balance of forces is primarily Coriolis and turbulent diffusion of momentum. (From Morison JH, McPhee MG, Curtin T and Paulson CA (1992) The oceanography of winter leads. *Journal of Geophysical Research* 97: 11199–11218.)

If this lead number is small because the ice is moving rapidly or the salt flux is small, the pressure gradient term is not significant in [23]. In this forced convection case, illustrated in **Figure 2B**, the boundary layer behaves as in the horizontally homogeneous case except that salt is advected and diffused away from the lead in the turbulent boundary layer.

If the lead number is large because the ice is moving slowly or the salt flux is large, the pressure gradient term is significant. In this free convention case the salinity disturbance is not advected away, but builds up under the lead. This creates pressure imbalances that can drive the type of cellular motion shown in **Figure 2A**.

Figure 3 shows conditions for which the lead number is unity for a range of ice thickness. Here the salt flux has been parametrized in terms of the air–sea temperature difference, and stress has been parametrized in terms of U_i. The figure shows the locus of points where L_0 is equal to unity. For typical winter and spring conditions, L_0 is close to 1, indicating that a mix of free and forced convection is common. Conditions where lead convection features have been observed are also shown in **Figure 3**. Most of these are in the free convection regime, probably because they are more obvious during quiet conditions.

There have been several dedicated efforts to study the effects of wintertime lead convection. The most recent example was the 1992 Lead Experiment (LeadEx) in the Beaufort Sea. **Figure 4** illustrates the average salinity profile at 9 m under a nearly stationary lead. The data was gathered with an autonomous underwater vehicle. Using the vehicle vertical motion as a proxy for vertical water velocity, it is also possible to estimate the salt flux $w'S'$. The lead was moving at $0.04\,m\,s^{-1}$, and estimates of salt flux put L_0 between 4 and 11 (free convection in **Figure 3**). Salinity increased in the downstream direction across the lead and reached a sharp maximum at the

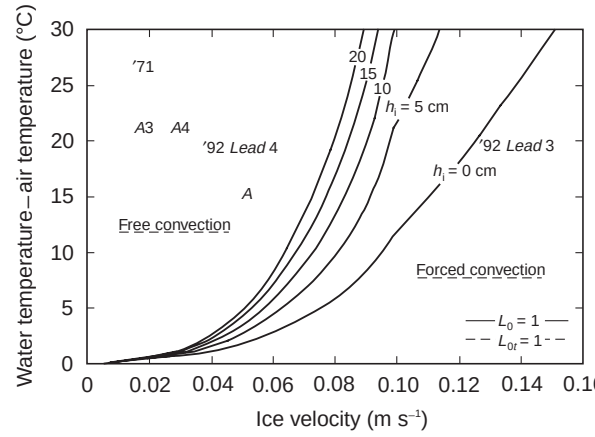

Figure 3 Air–water temperature difference versus U_i for L_0 equal to 1 for various ice thicknesses, h_i. Also shown are the temperature difference and ice velocity values for several observations of lead convection features such as underice plumes. Most of these are in the free convection regime: '71 denotes the AIDJEX pilot study; A3 denotes the 1974 AIDJEX Lead Experiment – lead 3 (ALEX3); A4 denotes ALEX4; A denotes the 1976 Arctic Mixed Layer Experiment; and '92 Lead 4 denotes the 1992 LeadEx lead 4. LeadEx lead 3 ('92 Lead 3) was close to $L_0 = 1$. (From Morison JH, McPhee MG, Curtin T and Paulson CA (1992) The oceanography of winter leads. *Journal of Geophysical Research* 97: 11199–11218.)

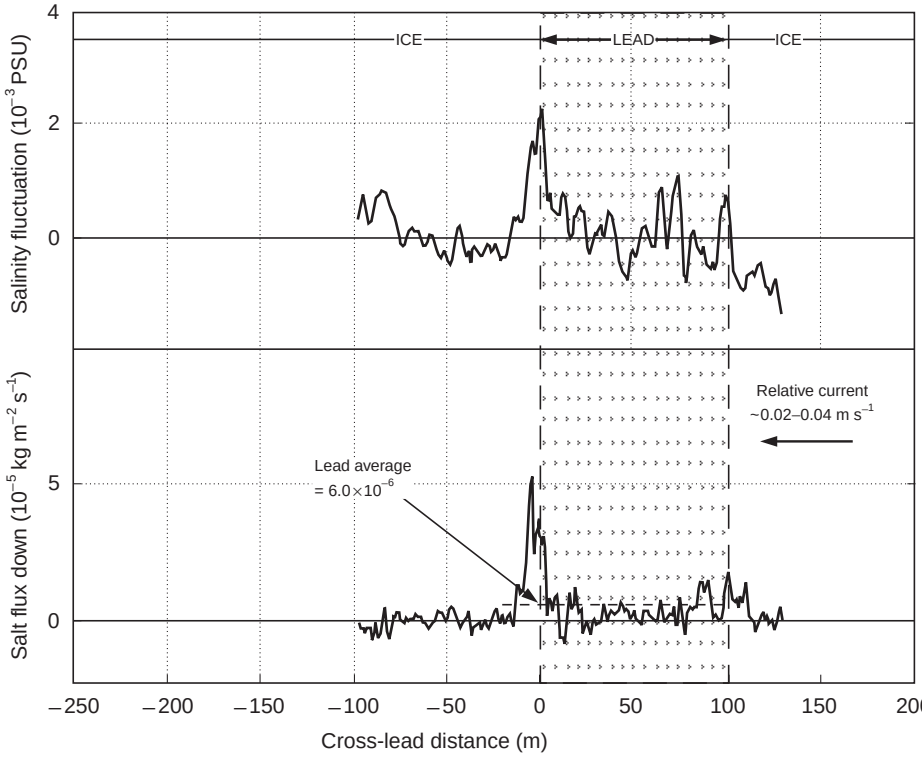

Figure 4 Composites of S' and $w'S'$ at 9 m depth measured with an autonomous underwater vehicle during four runs under lead 4 at the 1992 Lead Experiment. The horizontal profile data have been collected in 1 m bins. (From Morison JH, McPhee MG (1998) Lead convection measured with an autonomous underwater vehicle. *Journal of Geophysical Research* 103: 3257–3281.)

downstream edge. The salt flux was highest near the lead edges, but particularly at the downstream edge. With even a slight current, the downstream edge plume is enhanced by several factors. The vorticity in the boundary layer reinforces the horizontal density gradient at the downstream edge and counters the gradient at the upstream edge. The salt excess is greatest at the downstream edge by virtue of the salt that is advected from the upstream lead surface. The downstream edge plume is also enhanced by the vertical motion of water at the surface due to water the horizontal flow being forced downward under the ice edge.

Figure 5 shows the salt flux beneath a 1000 m wide lead moving at 0.14 m s^{-1} with L_0 equal to about 1 (**Figure 3**). Here the salt flux is more evenly spread under the lead surface. The salt flux derived from the direct $w'S'$ correlation method does show some enhancement at the lead edge. This may be partly due to the influence of pressure gradient forces and the reasons cited for the free convection case described above. The other factor that influences the convective pattern is the lead width. In the case of the 100 m lead in even a weak current, the convection may not be fully developed until the downstream edge is reached. For the 1000 m lead of the second case, the convection under the downstream portion of the lead was a fully developed unstable boundary layer. The energy-containing eddies filled the mixed layer and their dominant horizontal wavelength was equal to about twice the mixed layer depth.

Effects of Horizontal Inhomogeneity: Summertime Buoyancy Flux

The behavior of the boundary layer under summer leads is relatively unknown compared to the winter lead process. Because of the important climate consequences, it is a subject of increasing interest. Summertime leads are thought to exhibit a critical climate-related feature of air–sea–ice interaction, ice-albedo feedback. This is because leads are windows that allow solar radiation to enter the ocean. The proportion of radiation that is reflected (albedo) from sea ice and snow is high (0.6–0.9) while that from open water is low (0.1). The fate of the heat that enters summer leads is important. If it penetrates below the draft of the ice, it warms the boundary layer and is available to melt the bottom of the ice over a large area. If most of the heat is trapped in the lead above the draft of the ice, it will be available to melt small pieces of ice and the ice

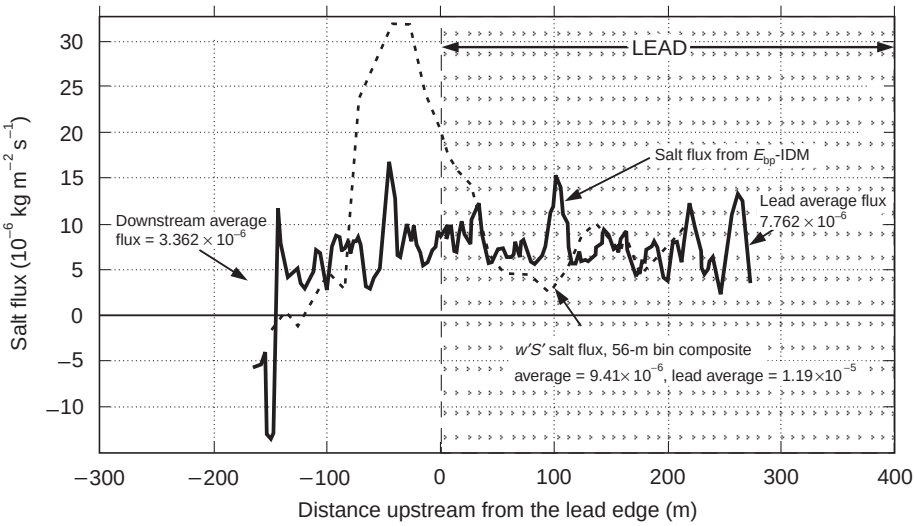

Figure 5 Composite average for autonomous underwater vehicle runs 1 to 5 at lead 3 of the 1992 Lead Experiment. The salinity is band-passed at 1 rad m^{-1} and is indicative of the turbulence level and is used to estimate the salt flux by the $E_{bp}-$IDM method of Morison and McPhee (1998). The salt flux is elevated in the lead and decreases beyond about 72 m downstream of the lead edge. The composite average of $w'S'$ in 56 m bins for the same runs is also shown in the center panel. The average flux and the decrease downstream are about the same as given by the $E_{bp}-$IDM method, but $w'S'$ suggests elevated fluxes near the lead edge. (From Morison JH, McPhee MG (1998) Lead convection measured with an autonomous underwater vehicle. *Journal of Geophysical Research* 103: 3257–3281.)

floe edges. In the latter case the area of ice will be reduced and the area of open water increased. This allows even more solar radiation to enter the upper ocean, resulting in a positive feedback. This process may greatly affect the energy balance of an ice-covered sea. The critical unknown is the partition of heating between lateral melt of the floe edges and bottom melt.

There are fundamental similarities between the summertime and wintertime lead problems. The equations of motion ([15]–[24]) are virtually identical. Only the sign of the buoyancy flux is opposite. The heat flux is important to summer leads and tends to decrease the density of the surface waters. However, as with winter leads, the buoyancy flux is controlled mainly by salt. As the top surface of the ice melts, much of the water that does not collect in melt ponds on the ice surface instead runs into the leads. If the ambient ice velocity is low, ice melt from the bottom surface will tend to flow upward and collect in the leads as well. Thus leads are the site of a concentrated flux of fresh water accumulated over large areas of ice. If this flux, F_S, into the lead is negative enough relative to the momentum flux represented by u_{*0}, the lead number, L_0, will be a large negative number and shear production of turbulent energy will not be able to overcome the stabilizing buoyant production. This means turbulent mixing will be weak beneath the lead surface and a layer of fresh water will accumulate near the surface of the lead. The stratification at the bottom of this fresh water layer may be strong enough to prevent mixing until a storm produces a substantial stress. This will be made even more difficult than in the winter situation because of the effect of stabilizing buoyancy flux on the boundary layer generally. The only way the fresh water will be mixed downward is by forced convection; there is no analogue to the wintertime free convection regime.

When there is sufficient stress to mix out a summertime lead, the pattern must resemble that of the forced convection regime in **Figure 2A**. At the upstream edge of the lead, fresh warm water will be mixed downward in an internal boundary layer that increases in thickness downstream until it reaches the steady-state boundary layer thickness appropriate for that buoyancy flux or the ambient mixed layer depth. The rate of growth should scale with the local value of u_{*0} (or perhaps $u_{*0}\eta_*$). At the downstream edge, another boundary layer conforming to the under-ice buoyancy flux and surface stress will begin to grow at a rate roughly scaling with the local u_{*0}. In spite of the generally stabilizing buoyancy flux, this process has the effect of placing colder, more saline water from under the ice on top of fresher and warmer (consequently lighter) water drawn from the lead. Thus, even embedded in the stable summer boundary layer, the horizontal inhomogeneity due to leads may create pockets of instability and more rapid mixing than might be expected on the basis of average conditions.

Recent studies of summertime lead convection at the 1997–98 Surface Heat Budget of the Arctic experiment saw the salinity decrease in the upper 1 m of leads to near zero and temperatures increase to more than 0°C. Only when ice velocities were driven by the wind to speeds of nearly $0.2\,\mathrm{m\,s^{-1}}$ were these layers broken down and the fresh, warm water mixed into the upper ocean. At these times the heat flux measured at 5 m depth reached values over $100\,\mathrm{W\,m^{-2}}$. The criteria for the onset of mixing are being studied along with the net effect of the growing internal boundary layers. Even with an understanding of the mixing process, it will be a challenge to apply this information to larger-scale models, because the mixing is nonlinearly dependent on the history of calm periods and strong radiation.

Internal Waves and Their Interaction with the Ice Cover

One of the first studies of internal waves originated with observations made by Nansen during his 1883 expedition. It did not actually involve interaction with the ice cover, but with his ship the *Fram*. He found that while cruising areas of the Siberian shelf covered with a thin layer of brackish water, the *Fram* had great difficulty making any headway. It was hypothesized by V. Bjerknes and proved by Ekman that this 'dead water' phenomenon was caused by the drag of the internal wave wake produced by the ship's hull as it passed through the shallow surface layer. This suggests that internal wave generation by deep keels may cause drag on moving ice. Evidence of internal wave generation by keels has been observed by several authors, but estimates of the amount of drag vary widely. This is due mainly to wide differences in the separation of the stratified pycnocline and the keels.

The drag produced by under-ice roughness of amplitude h_0 with horizontal wavenumber β moving at velocity V_i (magnitude v_i) over a pycnocline with stratification given by Brunt–Vaisala frequency, N, a depth d below the ice–ocean interface, can be expressed as an effective internal wave stress (eqn [25]), where C_wd (eqn [26]) accounts for the drag that would exist if there were no mixed layer between the ice and the pycnocline.

$$\Sigma_\mathrm{iw} = -\Gamma C_\mathrm{wd} V_\mathrm{i} \qquad [25]$$

$$C_\mathrm{wd} = \tfrac{1}{2}\beta_x^2 h_0 [(\beta_\mathrm{c}^2/\beta_x^2) - 1]^{1/2} \qquad [26]$$

The wavenumber in the direction of the relative ice velocity, V_i, is β_x, and β_c is the critical wave number above which the waves are evanescent ($\beta_\mathrm{c} = N/v_\mathrm{i}$). Γ is an attenuation factor that accounts for the separation of the pycnocline from the ice by the mixed layer of depth d (eqn [27]).

$$\Gamma = \left(\sinh^2(\beta d)\left\{\left[\coth(\beta d) - \frac{\beta \Delta b}{v_\mathrm{i}^2 \beta_x^2}\right]^2 + \frac{N^2}{v_\mathrm{i}^2 \beta_x^2} - 1\right\}\right)^{-1} \qquad [27]$$

Δb is the strength of the buoyancy jump at the base of the mixed layer. For wavenumbers of interest and d much bigger than about 10 m, Γ becomes small and internal wave drag is negligible. Thus it is not a factor in the central Arctic over most of the year. However, in the summer pack ice, and many times in the marginal ice zone, stratification will extend to or close to the surface. Then internal wave drag can be at least as important as form drag.

The ice cover also uniquely affects the ambient internal wave field. In most of the world ocean the internal wave energy level, when normalized for stratification, is remarkably uniform. It has been established by numerous studies that the internal wave energy in the Arctic Ocean is typically several times lower. In part this may be due to the absence of surface gravity waves. The other likely reason is that friction on the underside of the ice damps internal waves. Decomposing the internal wave field into vertical modes, one finds the mode shapes for horizontal velocity are a maximum at the surface. This is perfectly acceptable in the open water situation. However, at the horizontal scales of most internal waves, an ice cover imposes a surface boundary condition of zero horizontal velocity. The effect of this can be estimated by assuming that a time-varying boundary layer is associated with each spectral component of the internal wave field. This is not rigorously correct because all the modes interact in the same nonlinear boundary layer, and are thereby coupled. However, in the presence of a dominant, steady current due to ice motion, the effect on the internal wave modes can be linearized and considered separately. The near-surface internal wave velocity can be approximated as a sum of rotary components (eqn [28]).

$$V(z) = \sum_{n=0}^{M} D_n(z) \mathrm{e}^{\mathrm{i}\omega_n t} = \sum_{n=0}^{M} [A_n(z) + \mathrm{i}B_n(z)]\mathrm{e}^{\mathrm{i}\omega_n t} \qquad [28]$$

The internal wave motion away from the boundary $D_{\infty n}$ can be subtracted from the linear

time-varying boundary layer equation (eqn [1] with the addition of the time variation acceleration, $\partial V/\partial t$). This yields an equation for each rotary component of velocity in the boundary layer (eqn [29]).

$$i(\omega_n + f)(D_n - D_{\infty n}) = \frac{\partial}{\partial z} K \frac{\partial D_n}{\partial z} \qquad [29]$$

$$D_n = 0 \quad \text{at } z = z_0$$

$$D_n = D_{\infty n} \quad \text{at } z = d$$

This oscillating boundary layer equation can be solved for K of the form $K = ku_{*0}z\exp(-6|\omega + f|z/u_{*0})$. When we do this for representative internal wave conditions in the Arctic and compute the energy dissipation, we find the timescale required to dissipate the internal wave energy through under-ice friction is 32 days. This is a factor of 3 smaller than is typical for open ocean conditions. Assuming a steady state with internal wave forcing and other dissipation mechanisms in place, the under-ice boundary layer will result in a 75% reduction in steady-state internal wave energy. This suggests the effect of the under-ice boundary layer is critical to the unique character of internal waves in ice-covered seas.

Outstanding Issues

The outstanding issue of ice–ocean interaction is how the small-scale processes in the ice and at the interface affect the exchange between the ice and water. This is arguably most urgent in the case of heat and salt exchange during ice growth. When we apply laboratory-derived concepts for the diffusion of heat and salt to the ice–ocean interface, we get results that are not supported by observation, such as spontaneous frazil ice formation and large ocean heat flux under thin ice.

These results are causing significant errors in large-scale models. They stem from a molecular sublayer model of the ice–ocean interface (**Figure 1**) and the difference between the molecular diffusivities of heat and salt. What seems to be wrong is the molecular sublayer model. Recent results in the microphysics of ice growth reveal that the structure and thermodynamics of the growing ice produce instabilities and convection within the ice and extending into the water. The ice surface is thus not a passive, smooth surface covered with a thin molecular layer. Rather it is field of jets emitting plumes of supercooled, high-salinity water at a very small scale. This type of unstable convection likely tends to equalize the diffusion of heat and salt relative to the apparently unrealistic parameterizations we are using now.

Similarly, we do not really understand how the turbulent stress we might measure in the surface layer is converted to drag on the ice. Certainly a portion of this is through viscous friction in the molecular sublayer. However, in most cases the underside of the ice is not hydrodynamically smooth, which suggests that pressure force acting on the bottom roughness elements are ultimately transferring a large share of the momentum. Understanding this will require perceptual breakthroughs in our view of how turbulence and the mean flow interact with a rough surface buried in a boundary layer. Achieving this understanding is complicated greatly by a lack of contemporaneous measurements of turbulence and under-ice topography at the appropriate scales. This drag partition problem is general and not limited to the under-ice boundary layer. However, the marvelous laboratory that the under-ice boundary layer provides may be the place to solve it.

See also

Coupled Sea Ice–Ocean Models. Internal Waves. Sea Ice: Overview; Variations in Extent and Thickness. Sub Ice-shelf Circulation and Processes. Under-ice Boundary Layer.

Further Reading

Johannessen OM, Muench RD and Overland JE (eds) (1994) *The Polar Oceans and Their Role in Shaping the Global Environment: The Nansen Centennial Volume*. Washington, DC: American Geophysical Union.

McPhee MG (1994) On the turbulent mixing length in the oceanic boundary layer. *Journal of Physical Oceanography* 24: 2014–2031.

Morison JH, McPhee MG and Maykutt GA (1987) Boundary layer, upper ocean and ice observations in the Greenland Sea marginal ice zone. *Journal of Geophysical Research* 92(C7): 6987–7011.

Morison JH and McPhee MG (1998) Lead convection measured with an autonomous underwater vehicle. *Journal of Geophysical Research* 103(C2): 3257–3281.

Smith WO (1990) (ed.) *Polar Oceanography*. San Diego, CA: Academic Press.

Wettlaufer JS (1999) Ice surfaces: macroscopic effects of microscopic structure. *Philosophical Transactions of the Royal Society of London A* 357: 3403–3425.